Polarized infrared reflectivity of Cu_2CdSnS_4 single crystals

I. V. Bodnar[1], I. A. Victorov[2], A.G. Karosa[1], E.K. Arushanov[3], S. Levcenko[4*]

[1] Belarusian State University of Informatics and Radioelectronics, P. Brovka 6, 220013, Minsk, Belarus

[2] Scientific and Practical Materials Research Center of NAS of Belarus, P. Brovka 19, 220072, Minsk, Belarus

[3] Institute of Applied Physics, Academy of Sciences of Moldova, Academiei 5, MD, 2028, Chisinau, Republic of Moldova

[4] Felix-Bloch-Institut für Festkörperphysik, Universität Leipzig, Linnéstraße 5, 04103, Leipzig, Germany

*Corresponding author: S. Levcenko; email sergiu.levcenco@uni-leipzig.de

A polarization dependent infrared reflectivity study on oriented single crystal in the range of 100 – 500 cm^{-1} was performed to investigate the optical phonon modes in the stannite Cu_2CdSnS_4 semiconductor. Based on the symmetry analysis and multi-oscillator model calculation we determine the parameters of B_2 and E polar modes. The values of high frequency ε_∞ and static ε_0 dielectric constant are 7.69 and 10.01 for **E||c** and 6.53 and 8.81 for **E⊥c** polarization directions.

Cd-alloying of kesterites $Cu_2ZnSn(S,Se)_4$ (CZTSSe) materials provides an alternative possibility to tune the band gap energy from 1.0 to 1.5 eV for photovoltaic [1-5] and photoelectrochemical water splitting [6] applications. Cu_2CdSnS_4 (CCTS) has gained attention as a nonlinear optical material for infrared applications [7] and absorber layer for thin film solar cells. [8] The initial efforts to improve Cd alloyed kesterites via processing optimization have been already made and resulted champion devices with efficiency ~ 12% have been demonstrated. [1, 5] A number of positive effects on microstructure, heterojunction band alignment, minority carrier lifetime and band tails in Cd-alloyed absorbers are revealed. [1, 2] It is expected that the disorder of the kesterite crystal lattice can be reduced by Cd incorporation as less Zn atoms are involved in Cu_{Zn} and Zn_{Cu}

antisite defects and, consequently, the optoelectronic properties of the absorber material can be significantly improved. [9] To date, the lack of the basic material properties due to the difficulties of high crystalline fabrication hinders a detailed exploitation of this material. For example, the knowledge of the vibrational properties of Cu_2CdSnS_4 is still limited to the reference dataset from the far infrared (IR) absorption study on powders published in 1991 by M. Himmrich and H. Haeuseller [10] and some recent Raman scattering characterizations on polycrystalline powders and thin films. [3, 4, 8, 11] To get a more accurate and reliable information of the CCTS phonon spectra we present and analyze polarization dependent infrared reflectivity in the range of 100 – 500 cm^{-1} measured on the oriented CCTS single crystal grown by chemical vapor transport. The values of high frequency and static dielectric constant are also determined from the dispersion analysis of the infrared reflectivity.

To prepare CCTS single crystals we used a two-step growth process. In the first step, the CCTS polycrystalline compound was synthesized by the one-temperature method. The >99.99%-pure elemental components (copper, cadmium, tin and sulfur) weighted in ratios corresponding to the stoichiometric composition were loaded into a quartz ampoule, which was subjected to chemical - thermal treatment (etching in a mixture of acids HNO_3: HCl = 1: 3, washed in distilled water and annealed in vacuum at 1273 K). After evacuation to a residual pressure of about 10^{-3} Pa the ampoule was sealed off and placed into a vertical single zone furnace. The furnace was initially heated to ~870 K with a rate of ~50 K h^{-1} and kept at this level for ~2 h to provide homogenization of the melt. Then the temperature was elevated to ~1200 K with a same rate of ~50 K h^{-1} and annealed again at this level for ~2 h. Following this annealing, we conducted a planar crystallization of the melt by lowering the temperature of the furnace with a rate of ~50 K h^{-1} down to 1020 K. To homogenize the ingots, we annealed them at the same temperature for 240 h and turned the furnace off.

In the second step, the growth of single crystals was carried out in the quartz ampoule loaded with iodine and the grounded powder (~ 3 g) obtained from the polycrystalline ingots of the CCTS compound. The crystal growth occurred in a horizontal dual-zone furnace, where the temperature in the reaction zone was initially 100 K lower than in the crystallization zone. After a certain time, the temperature in the zones was equilibrated across the ampoule and was set to ~ 990 K, after which the temperature in the reaction zone was gradually increased over the course of 170 hours to 1070 - 1100 K. Then the furnace was turned off and the crystals were cooled down to room temperature. As the result the plate-like single crystals with mirror like (112) surface from one side with up to 9 × 2.5 mm^2 in area and 0.5 mm in thickness and crystal orientation along $[\bar{1}10]$ were grown. The composition of the grown single crystals was determined using microprobe X-ray spectral analysis. The electron beam of a Stereoscan-360 scanning electron microscope was used as an X-ray radiation source and an AVALON-8000 X-ray spectrometer served as an X-ray spectrum analyzer. The obtained composition of CCTS single crystals is Cu: Cd: Zn: S = 25.5: 12.7: 12.2: 49.6, which is in satisfactory agreement with the stoichiometric composition.

The structure and parameters of the unit cell of the obtained single crystals were determined by the X-ray method. The diffraction patterns were recorded on a DRON – 3 MX-ray diffractometer using CuKα radiation and a graphite monochromator. The results of X-ray studies are presented in Fig. 1. The diffraction pattern of CCTS shows that quaternary compound crystallizes in the stannite structure ($I\bar{4}2m$ space group) and contains Bragg reflexes characteristic of this crystal structure (ICDD (PDF2008), 00-029-0537). [12] The unit cell parameters calculated by the least squares method are - a = 5.585 ± 0.005 Å, c = 10.84 ± 0.01 Å and in agreement with earlier reported data but obtained with higher accuracy. [13]

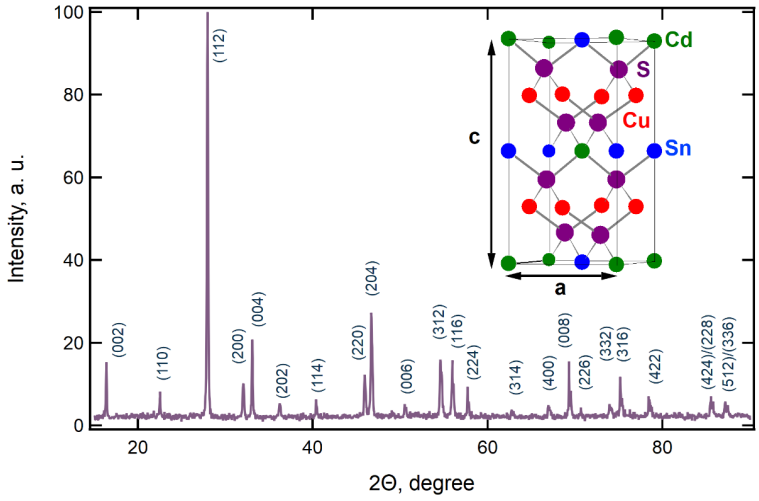

Fig. 1. XRD powder pattern of Cu_2CdSnS_4 single crystal. The inset displays the unit cell of Cu_2CdSnS_4 stannite structure.

IR reflection spectra are measured on the Fourier Nexus spectrometer (Thermo Nicolet), with a resolution of 2 cm^{-1}. For polarized IR measurements a gold wire grid polarizer placed in front of the sample and an aluminium mirror as reference sample are used. The angle of incidence of the light beam was below than 10°, near normal incidence to the crystal plane. The IR reflection spectra from (112) plane of Cu_2CdSnS_4 single crystals recorded for parallel (**E**||[$\bar{1}\bar{1}1$] or quasi-**E**||**c**) and perpendicular (**E**⊥**c**) polarizations in the range from 100 to 500 cm^{-1} are presented in Fig. 2 and 3, respectively. Insets of Fig. 2 and Fig. 3 show the schematic diagrams of the polarized IR experiment. The term quasi-**E**||**c** configuration is used as the polarization **E**||**c** is only partially realized (~ 65%) due to the θ angle of 36° between the vector of the electric field for the incident light (**E**) and the optical axis (**c**). [14] The pronounced six and four reflection bands can be clearly resolved in the parallel and perpendicular configurations (Figs. 2 and 3), respectively, which can be further examined.

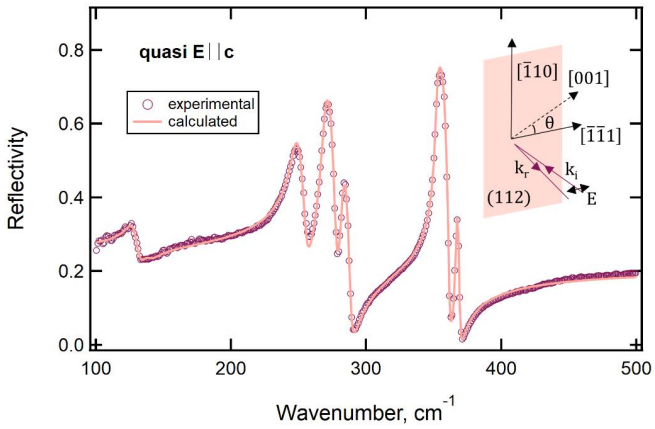

Fig. 2. Optical reflectivity for Cu_2CdSnS_4 single crystal with quasi **E‖c** polarization. The inset shows the experimental configuration used in the IR experiment, where $\mathbf{k_i}$ ($\mathbf{k_r}$) is the wave vector of the incoming (reflected) light beam at near incidence angle to (112) crystal plane, **E** is the electric field vector of the incoming polarized light and θ is the angle between the **c** axis and $[\bar{1}\bar{1}1]$ direction.

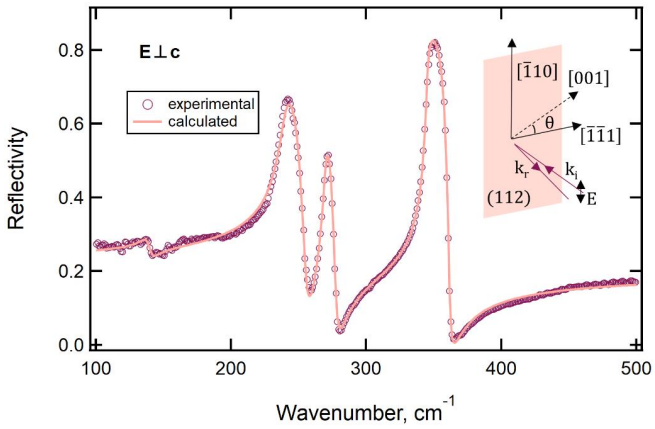

Fig. 3. Optical reflectivity for Cu_2CdSnS_4 single crystal with **E⊥c** polarization. The inset shows the experimental configuration used in the IR experiment, where $\mathbf{k_i}$ ($\mathbf{k_r}$) is the wave vector of the incoming (reflected) light beam at near incidence angle to (112) crystal plane, **E** is the electric field vector of the incoming polarized light and θ is the angle between the **c** axis and $[\bar{1}\bar{1}1]$ direction.

The irreducible representation for the zone-center (Γ point) phonon modes of CCTS is [10]:

$$\Gamma = 2A_1 + A_2 + 2B_1 + 4B_2 + 6E \quad (1)$$

where the polar B_2 and E modes are manifested in the IR and Raman spectra, the nonpolar A_1 and B_1 are active in Raman and A_2 is the silent mode. The polar modes measured from the (112) crystal plane depend differently on the polarization of the incident light relative to the **c** optical axis. [15] In particular, the B_2 modes are allowed in quasi-**E∥c** configuration, while the E modes are allowed in **E⊥c** polarization. These selection rules enable us to attribute the reflection bands in spectrum for **E⊥c** (Fig. 3) to E symmetry modes. However, the case of quasi-**E∥c** geometry (Fig. 2) becomes more complicated as besides the reflection bands originated from the B_2 modes a presence of some leaked E modes due to the imperfect **E∥c** polarization condition (θ ~36° angle between **E** and **c**) is also possible. [15] In fact, it can be seen in Fig. 2 that the number of the reflection bands is higher than the number of the B_2 modes theoretically expected (Eq. 1) for stannite CCTS.

To perform a more qualitative analysis of the IR spectra we employ a classical oscillator model that defined the complex dielectric function ε for an anisotropic uniaxial crystal as a sum of damped Lorentz oscillators [15, 16]

$$\varepsilon_{\perp}(\omega) = \varepsilon_{\perp\infty} + \sum_{j=1}^{n} \frac{s_{\perp j}\omega_{\perp j}^2}{\omega_{\perp j}^2 - \omega^2 - ib_{\perp j}\omega_{\perp j}\omega} \quad (2a)$$

$$\varepsilon_{\parallel}(\omega) = \varepsilon_{\parallel\infty} + \sum_{j=1}^{n} \frac{s_{\parallel j}\omega_{\parallel j}^2}{\omega_{\parallel j}^2 - \omega^2 - ib_{\parallel j}\omega_{\parallel j}\omega} \quad (2b)$$

with $\omega_{\perp j}$ ($\omega_{\parallel j}$) the transverse mode (TO) frequency of the lattice vibration, $b_{\perp j}$ ($b_{\parallel j}$) the damping constant, $s_{\perp j}$ ($s_{\parallel j}$) the oscillator strength of the j-th oscillator and $\varepsilon_{\perp\infty}$ ($\varepsilon_{\parallel\infty}$) the high frequency dielectric constant for **E⊥c** (**E∥c**) polarization, respectively. We analyze **E⊥c** configuration (inset

of Fig. 3) assuming pure $\varepsilon_{\perp}(\omega)$ dielectric function (Eq. 2a). For the case of the quasi-**E‖c** geometry (inset of Fig. 2), however, we consider a mixed dielectric function for uniaxial media [16]

$$\varepsilon_{\text{mix}}(\omega) = \frac{\varepsilon_{\perp}(\omega)\varepsilon_{\parallel}(\omega)}{\varepsilon_{\perp}(\omega)sin^2(\vartheta)+\varepsilon_{\parallel}(\omega)cos^2(\vartheta)} \quad (3)$$

where $\varepsilon_{\perp}(\omega)$ and $\varepsilon_{\parallel}(\omega)$ denote the dielectric function given in Eqs. (2a) and (2b) and ϑ =90-θ is the angle between the wave vector of the incoming light ($\boldsymbol{k}_i$) and the optical crystal axis **c**.

The reflectivity at normal incidence can be calculated from the complex dielectric function by using Fresnel equation:

$$R = \left|\frac{\sqrt{\varepsilon(\omega)}-1}{\sqrt{\varepsilon(\omega)}+1}\right|^2 \quad (4)$$

where $\varepsilon(\omega)$ is equal to $\varepsilon_{\perp}(\omega)$ and $\varepsilon_{\text{mix}}(\omega)$ for the **E⊥c** and quasi-**E‖c** polarization, respectively. To fit Eq. (4) to experimental IR data we applied a simulated annealing algorithm[17] and minimized the following cost function F :

$$F = \sum_{i=1}^{N}\left(R_i^{exp.} - R_i\right)^2 \quad (5)$$

where $R_i^{exp.}$ and R_i are the experimental and calculated reflectance values, respectively, and N is the number of experimental data points. In our evaluation routine we first determined the phonon parameters of $\varepsilon_{\perp}(\omega)$ from a fit to the IR spectrum for **E⊥c** polarization. Then, these parameter values were used as fixed one for fitting experimental IR data for quasi-**E‖c** polarization and extracting the phonon parameters of $\varepsilon_{\parallel}(\omega)$. The resulting theoretical reflectivity show a good agreement with experimental IR measurements (Fig. 2 and 3).

The longitudinal mode (LO) frequency of the polar mode can be determined as a frequency at which the energy loss function (imaginary part of -1/ε) has a maximum. [18] To visualize the split of TO and LO modes we compare the dielectric function and the energy loss function obtained

from the dispersion analysis on Fig. 4 and 5. Table I summarizes the determined values of TO and LO frequencies for polar B_2 and E modes observed in parallel and perpendicular polarizations.

TABLE I. Model parameter values.

Mode	ω_{TO} (cm^{-1})	ω_{LO} (cm^{-1})	b	s
		E‖c		
B_2^1	127 ± 1.5	130± 2	0.07 ±0.007	0.55 ± 0.02
B_2^2	266 ± 2	288 ± 3	0.017 ± 0.001	1.45 ± 0.02
B_2^3	360± 3	369 ± 3	0.005 ± 0.0006	0.32 ± 0.01
	$\varepsilon_{\infty\parallel}$=7.69 ± 0.09		$\varepsilon_{0\parallel}$=10.01 ± 0.14	
		E⊥c		
E^1	139± 2	140 ± 1.5	0.06 ± 0.01	0.13± 0.03
E^2	239 ± 2	255 ± 2	0.036 ± 0.002	1.40 ± 0.02
E^3	269 ± 3	278 ± 3	0.017± 0.001	0.25 ± 0.01
E^4	345 ± 3	361 ± 3	0.007 ± 0.0004	0.50 ± 0.01
	$\varepsilon_{\infty\perp}$=6.53 ± 0.08		$\varepsilon_{0\perp}$=8.81 ± 0.15	

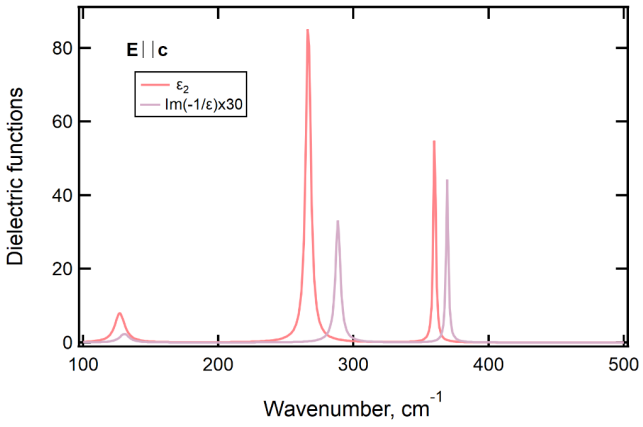

Fig. 4. Imaginary part of dielectric function (ε_2) and energy loss function (Im (-1/ε)) for Cu_2CdSnS_4 single crystal with **E‖c** polarization.

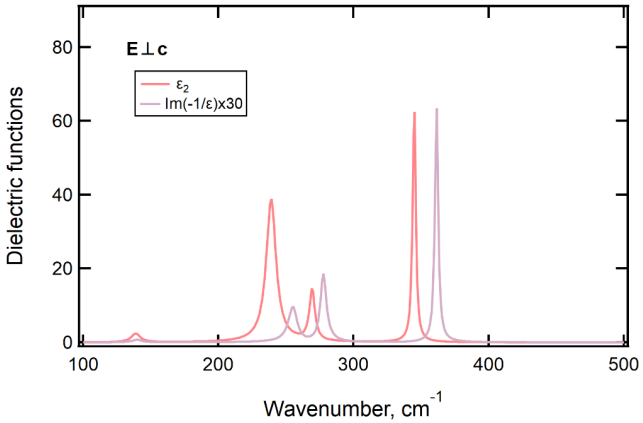

Fig. 5. Imaginary part of dielectric function (ε_2) and energy loss function (Im (-1/ε)) for Cu_2CdSnS_4 single crystal with **E⊥c** polarization.

Overall, we can identify 4 of 6 E modes and 3 of 4 B_2 modes predicted from group theory analysis for Cu_2CdSnS_4 compound. Based on the calculated zone center phonon frequencies for close related Cu_2ZnSnS_4 in stannite structure form, [19] we assume that the missing B_2 and two- E modes are located below 100 cm^{-1}. The evaluated TO polar modes are comparable to far -infrared absorption results, showing modes at 347, 271, 243, 139, 129 and 56 cm^{-1} for sintered powder samples, [10] and recent reports on Raman scattering characterization on polycrystalline powder [11] and thin films [8] and monograin powders [4]. Nevertheless, these earlier investigations were done on polycrystalline layers or under unpolarized light excitation, which limits study of the zone-center modes symmetry because of the randomly oriented grains in the probed specimens.

The high frequency dielectric constant shows appreciable anisotropic behavior and equal to 7.69 and 6.53 in **E‖c** and **E⊥c** polarization (Table I). This fact can be related to a structural effect on the electronic band structure of a stannite modification of the tetragonal crystal structure as it was theoretically predicted for Cu_2ZnSnS_4 semiconductor. [20] Moreover, it was calculated a higher value of ε_∞ in **E‖c** polarization in stannite Cu_2ZnSnS_4, [20] which is in agreement with our experimental result. Note that a different trend in ε_∞ for the chalcopyrites crystalizing in tetragonal

structure (space group $I\bar{4}2m$) was observed. [15, 21] It follows from Eqs. (2a) and (2b) that the static dielectric constant is $\varepsilon_0 = \varepsilon_\infty + \sum_{j=1}^{N} s_j$ and equals to 10.01 and 8.81 in **E**‖**c** and **E**⊥ **c** polarizations. The most intense B_2 (TO/LO) modes at 127/130 cm^{-1} and 266/288 cm^{-1} mainly contribute to $\varepsilon_{0\|}$, whereas the strong E (TO/LO) modes at 239/255 cm^{-1} and 345/361 cm^{-1} play a major role in $\varepsilon_{0\perp}$. We caution that these values of dielectric constants should be revised when the missing B_2 and E modes are identified in the IR spectra presumably in the low frequency range. [19] Finally, we checked the validity of the Lyddane-Sachs-Teller relations for uniaxial crystal [22]

$$\frac{\varepsilon_0}{\varepsilon_\infty} = \prod_{j=1}^{n} \left(\frac{\omega_{LO}}{\omega_{TO}}\right)^2 \quad (6)$$

and experimentally proved that left hand side and right hand side hold with a high accuracy for both polarization configurations and thus supporting our dispersion analysis of IR spectra.

In summary, we report a detailed study of polarized far infrared reflection of CCTS single crystals grown by chemical vapor technique with iodine as transport agent. A dispersion analysis is performed to quantify the transverse and longitudinal phonons of B_2 and E polar modes as well as the values of high frequency ε_∞ and static ε_0 dielectric constant for polarization along and perpendicular to the **c** optical axis.

This research is partially supported by the European Project INFINITE-CELL (Ref. H2020-MSCA-RISE-2017-777968, 2017–2021, www.infinitecell.eu). The authors appreciate also the financial support from bilateral project 19.80013. 01F/BL 16.02 and from the Institutional Project Nº CSSDT 15.817.02.04A. I.A.V. greatly acknowledges the support from the Fund of the Fundamental Investigations of Belarus, grant T19MLDG-003.

The data that support the findings of this study are available from the corresponding author upon reasonable request.

References

[1] C. Yan, K. Sun, J. Huang, S. Johnston, F. Liu, B. P. Veettil, K. Sun, A. Pu, F. Zhou, J. A. Stride, M. A. Green, and X. Hao , ACS Energy Lett. 2, 930 (2017).

[2] Z. Su , J.M.R. Tan , X. Li , X. Zeng, S. K. Batabyal, and L. H. Wong, Adv. Energy Mater. 5 1500682 (2015).

[3] Z. Y. Xiao, Y. F. Li, B. Yao, R. Deng, Z. H. Ding, T. Wu, G. Yang, C. R. Li, Z. Y. Dong, L. Liu, L. G. Zhang, and H. F. Zhao, J. Appl. Phys. 114, 183506 (2013).

[4] M. Pilvet, M. Kauk-Kuusik, M. Altosaar, M. Grossberg, M. Danilson, K. Timmo, A. Mere, and V. Mikli, Thin Solid Films 582,180 (2015).

[5] Z. Su, G. Liang, P. Fan, J. Luo, Z. Zheng, Z. Xie, W. Wang, S. Chen, J. Hu, Y. Wei, C. Yan, J. Huang, X. Hao, and F. Liu, Adv. Mater. 2020, 2000121 DOI: 10.1002/adma.202000121

[6] Y. F. Tay, H. Kaneko, S. Y. Chiam, S. Lie, Q. Zheng, B. Wu, S. S. Hadke, Z. Su, P. S. Bassi, D. Bishop , T. C. Sum, T. Minegishi, J. Barber, K. Domen, and L. H. Wong, Joule 2, 537 (2018).

[7] K. A. Rosmus, J. A. Brant, S. D. Winsneski, D. J. Clark, Y. S. Kim, J. I. Jang, C. D. Brunetta, J. H. Zhang, M. N. Srnec, and J. A. Aitken, Inorg. Chem. 53, 7809 (2014).

[8] S. Hadke, S. Levcenko, G. S. Gautam, C. J. Hages, J. A. Márquez, V. Izquierdo-Roca, E. A. Carter, T. Unold, and L. H. Wong, Adv. Energy Mater. 9, 1902509 (2019).

[9] G. S. Gautam, T. P. Senftle, and E. A. Carter, Chem. Mater. 30, 4543 (2018).

[10] M. Himmrich and H. Haeuseller, Spectrochim. Acta A 47, 933 (1991).

[11] M. Pilvet, M. Kauk-Kuusik, M. Grossberg, T. Raadik, V. Mikli, R. Traksmaa, J. Raudoja, K. Timmo, and J. Krustok , J. Alloys Compd. 723, 820 (2017).

[12] S. A. Kissin, D. R. Owens, and W. L. Roberts, Can. Mineral.16, 139 (1978).

[13] H. Matsushita, T. Ichikawa, and A. Katsui, J. Mater. Sci. 40, 2003 (2005).

[14] B. Tell, J. L. Shay, and H. M. Kasper, Phys. Rev. B 4, 2463 (1971).

[15] V. Riede, H. Sobotta, H. Neumann, and H. X. Nguyen, Solid State Commun. 28, 449 (1978).

[16] L. Merten and G. Lamprecht, Phys. Status Solidi 39, 573 (1970).

[17] A. Corana, M. Marchesi, C. Martini, and S. Ridella, ACM T. Math. Software 13, 262 (1987).

[18] J. P. van der Ziel, A. E. Meixner, H. M. Kasper and J. A. Ditzenberger, Phys. Rev. B 9 , 4286 (1974).

[19] T. Gurel, C. Sevik, and T. Cagın, Phys. Rev. B 84, 205201 (2011).

[20] C. Persson, J. Appl. Phys. 107, 053710 (2010).

[21] N. N. Syrbu, M. Bogdanash, V. E. Tezlevan, and I. Mushcutariu, Physica B 229, 199 (1997).

[22] W. Cochran and R. A. Cowley, J. Phys. Chem. Solids 23, 447 (1962).

PLEASE CITE THIS ARTICLE AS DOI: 10.1063/5.0024482

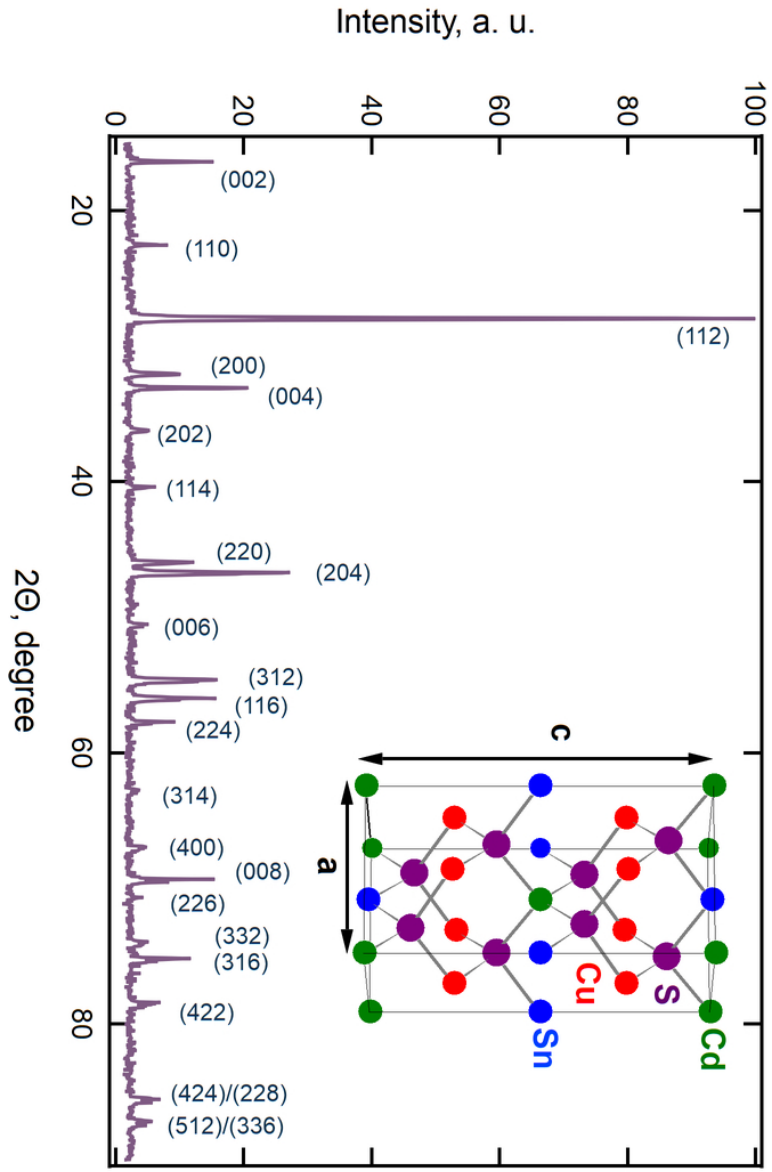

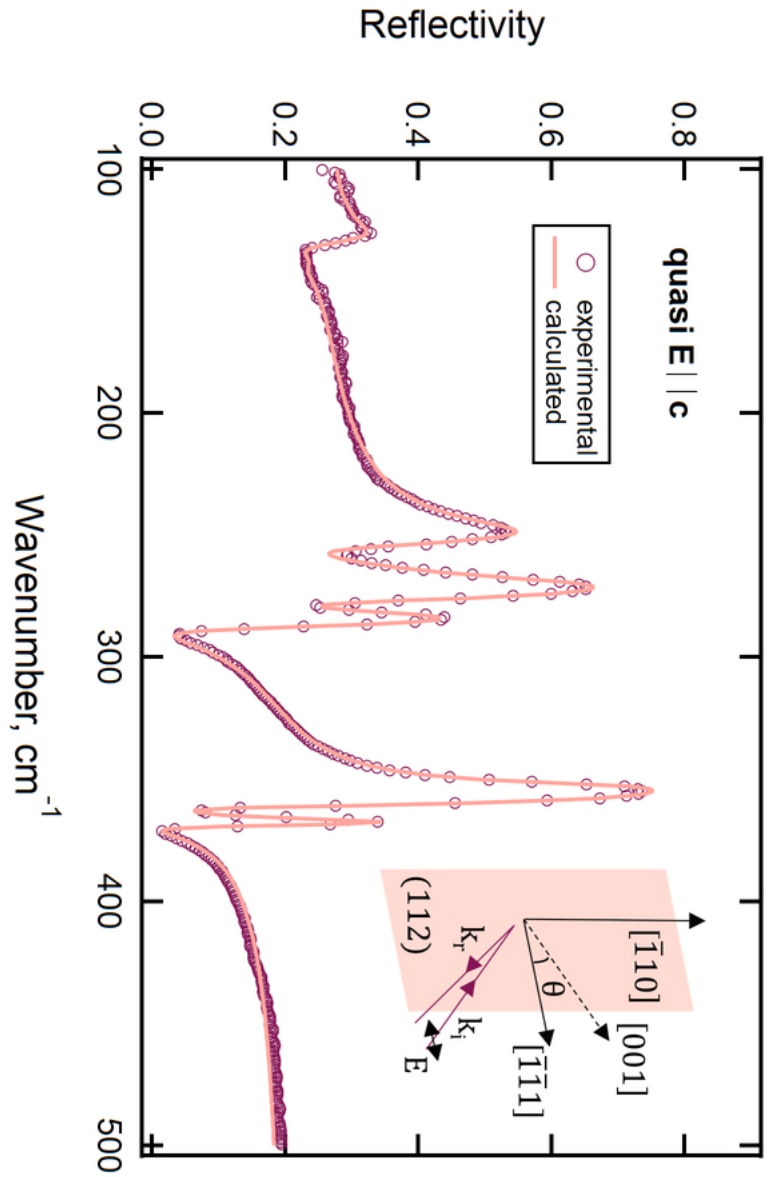

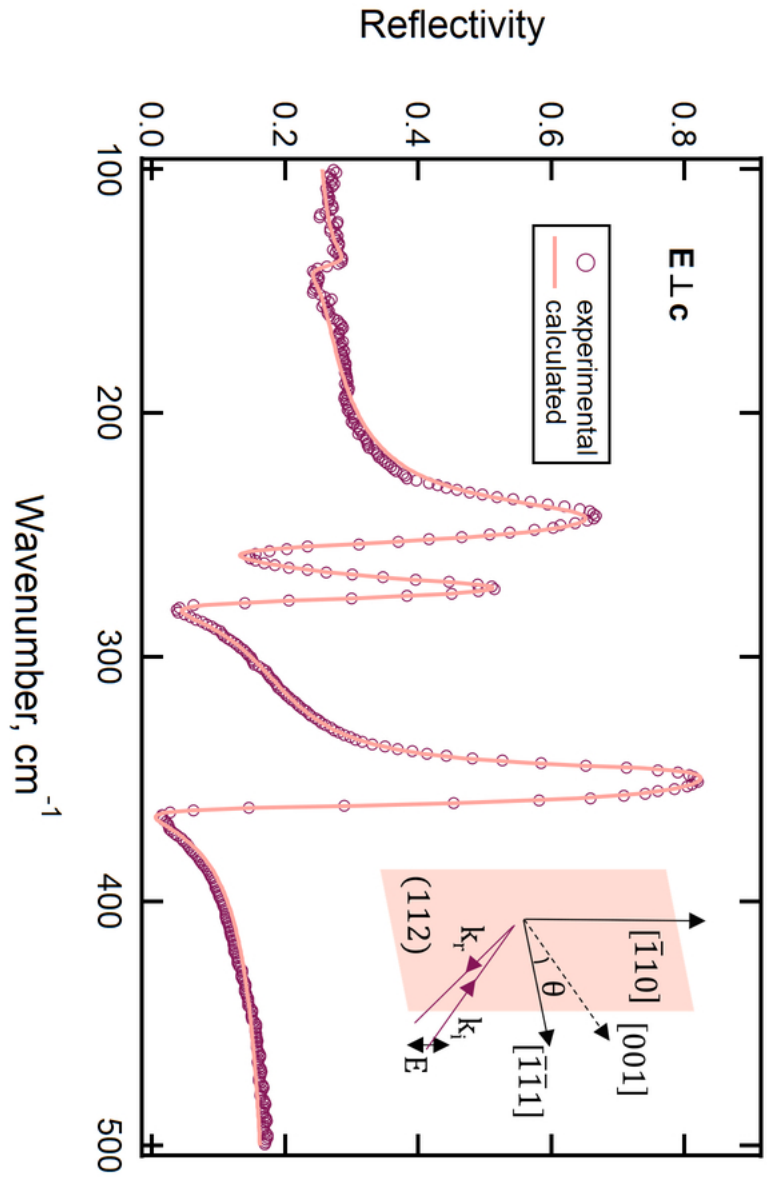

PLEASE CITE THIS ARTICLE AS DOI: 10.1063/5.0024482